RSC Advances




ROYAL SOCIETY OF CHEMISTRY

www.rsc.org/advances

**Colour graphic:**

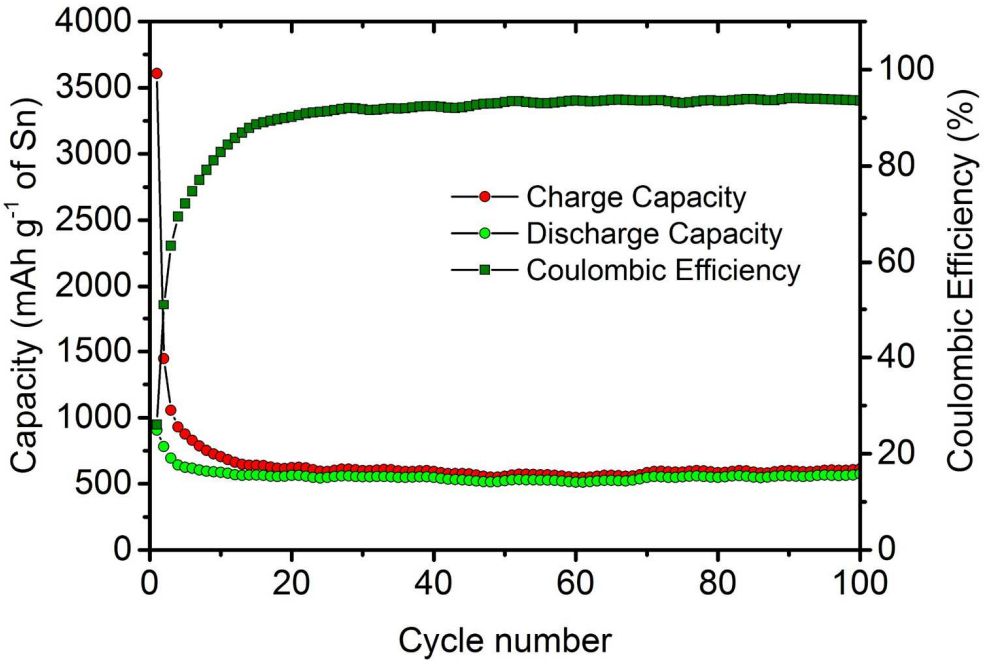


**Text: one sentence, of maximum 20 words, highlighting the novelty of the work.**

A 3D porous Ni/Sn-O-C composite thin film anode is electrodeposited from organic electrolyte containing LiPF6 and exhibits satisfactory electrochemical performance.

Journal Name

RSCPublishing

ARTICLE

# Three-dimensional porous nickel supported Sn-O-C composite thin film as anode material for lithium-ion batteries

Cite this: DOI: 10.1039/x0xx00000x

Received 00th January 2012,
Accepted 00th January 2012

DOI: 10.1039/x0xx00000x

www.rsc.org/

Xin Qian [a], Tao Hang [a,*], Guang Ran [b,*], Ming Li [a]

A three-dimensional porous nickel supported Sn-O-C composite thin film anode is fabricated by galvanostatical electrodeposition of active material Sn onto a patterned three-dimensional porous nickel current collector from organic electrolyte. The unique structure enables homogeneous coating of Sn-O-C composite thin film with 100 nm in thickness on highly porous dendritic Ni particles, along with the existence of inter-particle spacings, could efficiently accommodate great volume change caused by lithiation and delithiation of active material Sn. The morphology, crystalline structure and chemical composition of Sn-O-C composite are characterized by field emission scanning electron microscopy (FESEM), X-Ray diffraction (XRD), X-ray photoelectron spectroscopy (XPS) and transmission electron spectroscopy with an energy dispersive X-ray analyzer (TEM-EDX), respectively. The results demonstrate that the Sn-O-C composite is composed of agglomerated Sn nanocrystals inhomogeneously distributed in decomposition products of organic electrolyte. Moreover, the electrochemical behavior of the Sn-O-C composite anode is investigated by cyclic voltammetry (CV), galvanostatic charge/discharge tests and electrochemical impedance spectroscopy (EIS). This anode delivers a discharge capacity of 573.4 mAh (g of Sn)$^{-1}$ (0.0883 mAh cm$^{-2}$) after 100 cycles at 0.2 C-rate, and the augmentation in total SEI and interfacial charge transfer impedance well explained the gradual capacity fading as cycle number increases.

## Introduction

The great demand for high capacity, long cycle life lithium-ion batteries used in portable electronics and electric vehicles has prompted the research and development of non-carbonaceous anode materials.[1, 2] Tin has been proposed as one of the most proposing anode materials due to its high theoretical capacity ($Li_{4.4}Sn$, 994 mAh g$^{-1}$),[3] which is more than two times higher than that of commercial graphite anode ($LiC_6$, 372 mAh g$^{-1}$). However, pure tin anode suffers from rapid capacity fading and serious pulverization issues caused by great volume change (～300 %) during charge (lithiation)/discharge (delithiation) processes.[4, 5] In order to solve the problem, various attempts has been employed to accommodate the volume change of Sn, for the purpose to improve cycling stability.

To date, one strategy is to design substrate with micro/nano structure in order to enhance the adhesion strength between active material and current collector.[6-8] Another strategy is to fabricate Sn-based intermetallics to obtain improved electrochemical properties, such as Ni-Sn and Co-Sn electrodes.[9-12] The reason why Sn-based intermetallics could enhance electrochemical properties is that the other component acts as inactive buffering matrix to efficiently accommodate volume change when Sn and Li form $Li_xSn$ alloy in the charge process.[13] Besides, other attempts like mesoporous structure,[14] core-shell structure,[15] nanostructured Sn-based anode materials[16-18] have been reported.

Recently, Osaka et al. have electrodeposited core-shell structured Sn-O-C composite anode material on flat copper foil current collector from organic electrolyte.[19-23] The electrodeposition technique enables direct contact between Sn active material and current collector, and it exempts the use of conducting additive and polymer binder. The core-shell structured Sn-O-C composite anode prepared by electrodeposition from organic electrolyte containing $LiClO_4$ possesses discharge capacity of 465 mAh (g of Sn)$^{-1}$ with 80 % capacity retention after 100 cycles.[20] And the discharge capacity only remains 69 mAh (g of Sn)$^{-1}$ after 100 cycles when the Sn-O-C composte is electrodeposited from organic electrolyte containing $LiPF_6$.[23] However, the Sn-O-C composite film is easy to peel off from the flat copper current collector as the thickness of film increases, nevertheless, the poor reproducibility of core-shell structured Sn-O-C composite film also impedes its usage.

In this paper, we report a three-dimensional porous nickel supported Sn-O-C composite thin film by a two-step galvanostatical electrodeposition technique from organic electrolyte. The three-dimensional nano-metals (Ni or Cu) composed of numerous pores and dendritic walls have attracted tremendous attention because they can provide strong mechanical support, high surface area, short diffusion length for electrons and ions.[24-27] The highly porous structure with enhanced surface roughness could efficiently improve adhesion force between active material and substrate. In the meanwhile, we also conduct experiments to optimize the electrodeposition parameters for the purpose to achieve optimum

performance. Fig. 1 shows schematic of typical fabrication procedure of three-dimensional porous nickel supported Sn-O-C composite thin film. The design contains numerous size-fitted pores and dendrites with suited inter-spacing which could function as good buffer to accommodate volume change of active material during charge/discharge processes, as well as high surface area with enhanced roughness to improve adhesion force between Sn-O-C composite and current collector.

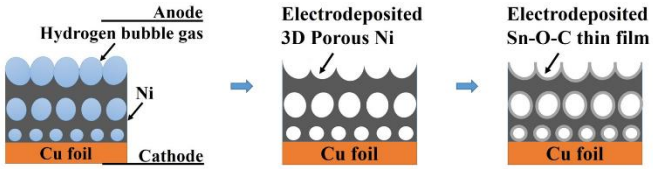


**Fig. 1** Schematic of typical fabrication procedure of three-dimensional porous nickel supported Sn-O-C composite thin film.

## Experimental

The preparation of three-dimensional porous nickel supported Sn-O-C composite thin film anode involved a two-step galvanostatical electrodeposition. All solvents and chemicals were of reagent quality without further purification. In the first step, three-dimensional porous nickel was electrodeposited on a flat copper foil with working area precisely controlled at 1.00 $cm^2$, and the other surface areas of the copper foil were covered by insulating tapes, the whole electrodeposition process was conducted in a electrolytic bath containing 2 mol $L^{-1}$ $NH_4Cl$ (Sinopharm Chemical Reagent, 99.5%) and 0.1 mol $L^{-1}$ $NiCl_2{\cdot}6H_2O$ (Sinopharm Chemical Reagent, 98.0%) at a pH value of 3.5 with a Pt counter electrode and Cu foil as a working electrode.[26, 28] The Cu foil was immersed in 20 v/v% $H_2SO_4$ for 10 s, rinsed with deionized water, and dried by the heater blower before electrodeposition. The electrodeposition parameter was controlled at a current density of 3.0 A $cm^{-2}$ for 60 s at room temperature, and the electrolyte was violently stirred by a magnetic stirrer during the process. Then the specimen was rinsed with deionized water, dried in vacuum chamber for 10 h and transferred to glove box filled with Ar atmosphere.

In the second step, the galvanostatical electrodeposition was conducted in a three-electrode electrolytic bath with 2.5 mmol $L^{-1}$ $SnCl_2$ (Alfa Aesar, 99%) dissolving in an ethylene carbonate (EC) : dimethyl carbonate (DMC) (1:1 v/v) electrolyte solution (Shenzhen Capchem Technology Co.,Ltd, water content less than 20 ppm) containing 1 mol $L^{-1}$ $LiPF_6$. Both the preparation of organic electrolyte and electrodeposition process were conducted in the glove box filled with Ar atmosphere with dew point below -100 °C. And the electrodeposition process was program controlled by electrochemical workstation (CHI660E, Chenhua, Shanghai) with a Pt quasi-reference electrode, a Pt counter electrode and a three-dimensional porous nickel as a working electrode. A constant cathodic current of 0.025 mA $cm^{-2}$ was applied to pass a charge of 0.25 C $cm^{-2}$ for galvanostatical electrodeposition of Sn-O-C composite thin film. After electrodeposition of Sn-O-C composite thin film, the specimen was rinsed with dimethyl carbonate and dried in vacuum chamber overnight for further electrochemical measurements and characterizations.

The three-dimensional porous nickel supported Sn-O-C composite thin film electrode was transferred into another three-electrode glass cell containg 1 mol $L^{-1}$ $LiPF_6$ electrolyte dissolved in EC : DMC (1:1 v/v) (Shenzhen Capchem Technology Co.,Ltd, water content less than 20 ppm). The galvanostatic charge/discharge tests were evaluated with a battery testing system (Kejing, Shenzhen) at room temperature using lithium metal foil as reference and counter electrode, and the as-prepared Sn-O-C composite thin film electrode as working electrode. The current density was controlled at 0.045 mA $cm^{-2}$ (0.2 C) in the potential range between 0.01 V and 1.50 V vs. $Li/Li^+$. In order to highlight the promotion effect of 3D highly porous dendritic structure on capacity retention, bare Sn-O-C composite on simple flat Cu substrate is also synthesized and galvanostatically charged/discharged under the same experimental conditions with 3D porous nickel supported Sn-O-C thin film anode. Furthermore, both cyclic voltammetry (CV) and electrochemical impedance spectroscopy (EIS) were carried out on 3D porous nickel supported Sn-O-C thin film anode with an electrochemical workstation (CHI660E, Chenhua, Shanghai) at room temperature. The CV measurement was conducted in a potential window of 0.01-1.50 V vs. $Li/Li^+$ at a scan rate of 0.1 mV $s^{-1}$, and the EIS was measured at open circuit voltage upon reaching a full charge at 0.01 V vs. $Li/Li^+$ with 10 mV voltage amplitude and a frequency range between 1 MHz and 0.01 Hz.

Filed emission scanning electron microscopy (FESEM, Siron 200) equipped with an energy dispersive X-ray analyzer (EDX) was performed to analyze the surface morphology and chemical composition of the as-prepared Sn-O-C composite thin film. X-ray diffraction (XRD) was carried out by Ultima IV equipped with Cu Kα (λ=0.1541 nm) radiation, the scanning range (2θ) was from 20° to 80° and scanning speed was 5° $min^{-1}$. The electrodeposited three-dimensional porous nickel supported Sn-O-C composite thin film was characterized by X-ray photoelectron spectroscopy (XPS, Axis Ultra Dld) in order to analyze the elemental composition and existing state. In the end, the crystallographic structure of as prepared Sn-O-C composite was characterized by transmission electron spectroscopy with an energy dispersive X-ray analyzer (TEM-EDX, JEM 2010).

## Results and Discussion

Fig. 2 (a)-(c) show the SEM images of the electrodeposited three-dimensional porous nickel at different magnifications. A top view in Fig. 2 (a) clearly shows that the porous nickel contains numerous homogeneously distributed pores and network of walls. And the inset graph in Fig. 2 (a) shows the cross-sectional SEM image of three-dimensional porous nickel, it demonstrates that the walls are composed of numerous dendrites and the thickness of porous nickel is approximately 20 μm. Fig. 2 (b) shows that the average diameter of these pores is approximately 8 μm and the dendritic walls are composed of Ni particles with different inter-particle spacings. Fig. 2 (c) shows the magnified SEM image of Ni particles with feature size ranging from several hundreds of nanometers to about one micrometer in diameter, and it appears to suggest that the existence of inter-particle spacing can efficiently accommodate serious volume change of active materials during charge/discharge tests.

After electrodeposition of Sn-O-C composite thin film, the specimen was rinsed with DMC and dried for SEM investigation. Fig. 2 (d)-(f) show the SEM images of the three-dimensional porous nickel supported Sn-O-C composite thin film. Fig. 2 (d) is the top view SEM image, the inset graph is the cross-sectional SEM image, but no obvious change can be seen compared to Fig. 2 (a). Fig. 2 (e) shows that the average diameter of these pores remains approximately 8 μm without



 

any obvious change compared with Fig. 2 (b). However, compared with Fig. 2 (c), a homogeneous thin film attached to the surface of highly porous dendritic Ni particles can be seen from Fig. 2 (f), which is the electrodeposition result from organic electrolyte.

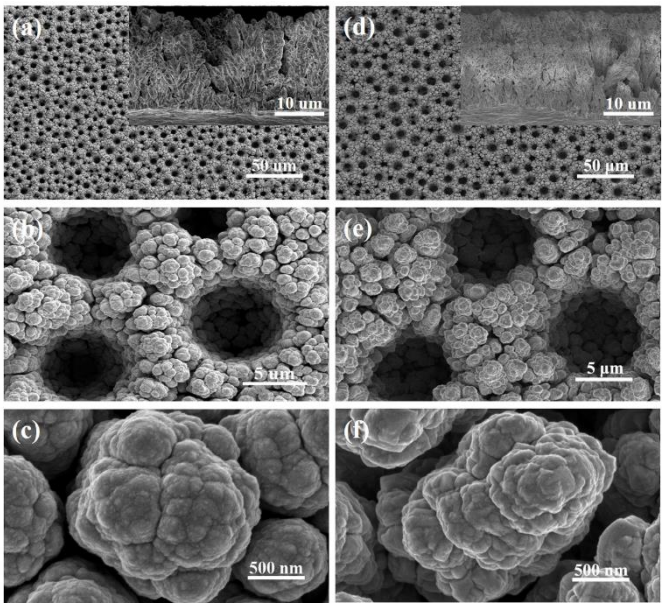


**Fig. 2** Top view SEM images of surface morphologies of electrodeposited three-dimensional porous nickel (a) (inset graph is cross-sectional SEM image), (b), (c) and three-dimensional porous nickel supported Sn-O-C composite thin film (d) (inset graph is cross-sectional SEM image), (e), (f).

The XRD patterns of three-dimensional porous nickel supported Sn-O-C composite thin film is shown in Fig.3 (a). The peaks belonging to tetragonal phase of tin are observed with 2θ values of 30.64º, 31.99º, 55.29º, 62.53º, 63.79º, 64.58º, 72.34º, 73.18º and 79.44º, which correspond to the 200, 101, 301, 112, 400, 321, 222, 411 and 420 crystal planes of β-tin (JCPDS # 04-0673), respectively. The other peaks appeared in XRD pattern belongs to three-dimensional porous Ni and Cu substrate. XPS measurement is also carried out to further analyze the composition and constitution of the as-prepared material.However, due to the fact that XPS analysis only reveals elemental composition of the composite within several nanometers beneath the surface, in order to avoid misconception caused by surface oxidation of the material, the XPS measurement is conducted after etching for three minutes (the etching depth is about 8 nm) and the spectra are shown in Fig. 3 (b)-(c). Peaks correspond to $C_{1s}$, $O_{1s}$, $Sn_{3d5/2}$ and $Sn_{3d3/2}$ are observed. A peak located at the binding energy about 284.7 eV is observed in the spectrum of $C_{1s}$ shown in Fig. 3 (b), which represents the electronic state of carbon is C-C bond.[29] A peak at about 531.9 eV is observed in the spectrum of $O_{1s}$ shown in Fig. 3 (c), which represents the oxygen is supposed to exist in the state of C-O-C. In Fig.3 (d), peaks located at 485.0 eV and 493.4 eV correspond to $Sn_{3d5/2}$ and $Sn_{3d3/2}$, respectively. The spectrum of $Sn_{3d5/2}$ indicates that the electronic state of Sn is Sn-Sn bond, because the peak of 485.0 eV accords with Sn metal. Considering the result of XRD that Sn exists in tetragonal phase which corresponds to Sn crystals, a conclusion can be safely drawn that the only crystalline phase is Sn metal. Furthermore, the decomposition of organic electrolyte during galvanostatical electrodeposition of the deposit results in the formation of C-C and C-O-C bonds. Therefore, XPS analysis reveals that the deposit is composed of Sn crystals inhomogeneously distributed in decomposition products of organic electrolyte.

The three-dimensional porous nickel supported Sn-O-C composite thin film is directly electrodeposited on the copper wire mesh for TEM investigation. Fig. 4 (a) shows the elemental analysis of the deposit performed by EDX equipped in TEM, the result indicates that elemental Sn, O and C are detected. Then, the structure of electrodeposited Sn-O-C composite is investigated by TEM image, as shown in Fig. 4 (b). A continuous thin film attached to the surface of porous nickel with approximate 100 nm in thickness can be clearly observed,

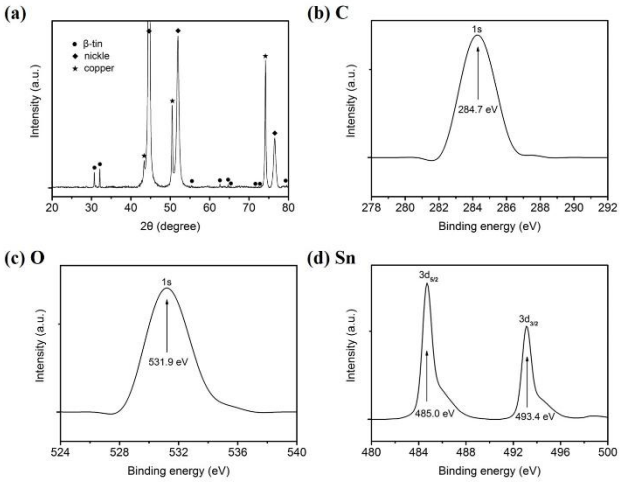


**Fig. 3** (a) XRD pattern of the as-prepared Sn-O-C composite thin film; (b), (c), (d) correspond to XPS spectra of $C_{1s}$, $O_{1s}$ and $Sn_{3d5/2}$ after etching for 3 minutes, respectively.

and agglomerated tiny Sn particles with irregular shapes and different sizes are inhomogeneously distributed in the Sn-O-C composite, as represented in the dark areas (not substrate). The inset graph shows the selected area electron diffraction (SAED) pattern of circle area highlighted with white solid line in Fig. 4 (b). The diffraction ring in SAED pattern shows characteristics of both amorphous and polycrystalline substances. The diffuse central spot is diffraction result of amorphous decomposition products of organic electrolyte, and the diffuse diffraction rings imply a polycrystalline Sn phase but with characteristic size of Sn crystal at about several nanometers, here we refer to it as Sn nanocrystal. Therefore, the electrodeposited Sn-O-C composite thin film is composed of agglomerated Sn nanocrystals inhomogeneously distributed in amorphous decomposition products of organic electrolyte, which can be further proved by the HRTEM analysis in the previous work reported in reference.[20] And the amorphous decomposition products could function as good buffer to accommodate volume change of active material Sn during charge/discharge tests.

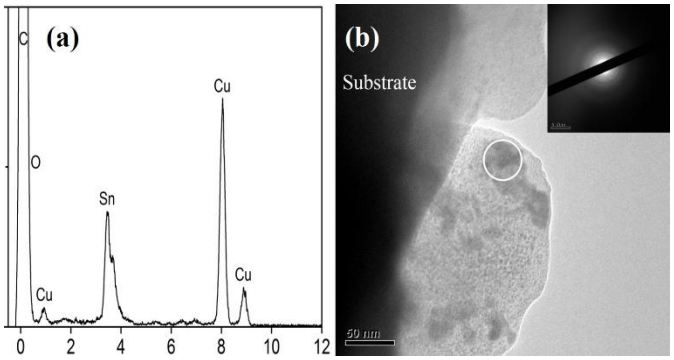


**Fig. 4** (a) EDX analysis and (b) TEM image (inset graph is SAED pattern of circle area in (b)) of three-dimensional porous nickel supported Sn-O-C composite thin film.

The electrochemical cycling performance and coulombic efficiency of the three-dimensional porous nickel supported Sn-O-C composite thin film anode measured by galvanostatical charge/discharge tests at a current density of 0.045 mA $cm^{-2}$ (0.2 C) is shown in Fig. 5 (a). The charge/discharge capacities are calculated based on the assumption that all the passed charges are used to reduce $Sn^{2+}$ to Sn metal, thus the net mass of Sn is 0.154 mg. The first cycle delivers a charge/discharge capacity of 3605.8 mAh (g of Sn)$^{-1}$ (0.5553 mAh $cm^{-2}$) and 940.3 mAh (g of Sn)$^{-1}$ (0.1448 mAh $cm^{-2}$), respectively. The extremely high charge capacity and low coulombic efficiency (26.1 %) in the first cycle is due to further reduction of oxidized state of active material Sn and solid electrolyte interphase (SEI) formation.[30, 31] After first cycle, the discharge capacity decreases rapidly until reaching a steady value about 590.9 mAh (g of Sn)$^{-1}$ (0.091 mAh $cm^{-2}$) at 8$^{th}$ cycle, while the coulombic efficiency gradually increases to 79% at 8$^{th}$ cycle. Afterwards, the discharge capacity keeps relatively steady despite of an infinitesimal decrease as cycle number increases, it remains a value as high as 573.4 mAh (g of Sn)$^{-1}$ (0.0883 mAh $cm^{-2}$) at 100$^{th}$ cycle with discharge capacity retention rate of 61 %. On the other hand, the coulombic efficiency rises to 90 % at 18$^{th}$ cycle and keeps steady at about 93.5% in the following cycles with an uttermost value of 95.5%. The high discharge capacity retention of the Sn-O-C composite thin film anode is attributed to the highly porous dendritic structure of Ni with high surface roughness, which not only enhances the adhesion force between active material and current collector but also functions as good buffer to accommodate volume change during charge/discharge tests.

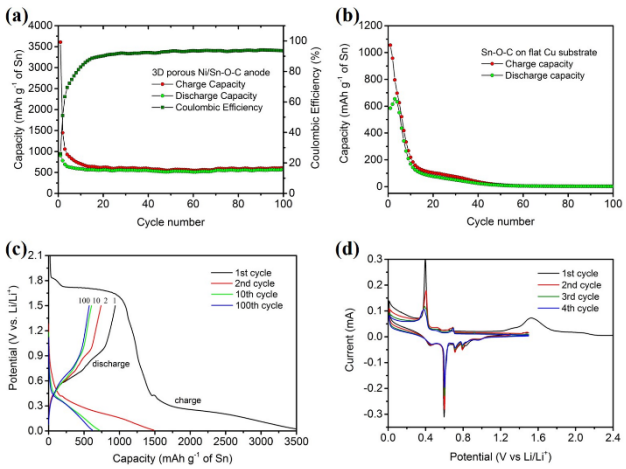


**Fig. 5** (a), (b): Cycling performance of 3D porous Ni/Sn-O-C thin film anode and bare Sn-O-C composite on simple flat Cu substrate with a current density of 0.045 mA $cm^{-2}$, respectively; (c) Charge/discharge potential profiles of 3D porous Ni/Sn-O-C anode between 0.01 V and 1.50 V vs. Li/$Li^+$; (d) CV profiles of the anode in a potential window between 0.01 V and 1.50 V vs. Li/$Li^+$ at a scan rate of 0.1 mV $s^{-1}$ at the first four cycles.

In order to validate the fact that 3D highly porous dendritic structures can accommodate volume change during charge/discharge tests and improve the capacity retention, bare Sn-O-C on simple flat Cu substrate is also electrochemically cycled at the same current density for comparison purpose. The charge and discharge capacity are both shown in Fig. 5 (b). It is obvious that the bare Sn-O-C on flat Cu substrate exhibits really poor electrochemical performance. This anode delivers a passable charge capacity of 1054 mAh (g of Sn)$^{-1}$ (0.1624 mAh $cm^{-2}$) and discharge capacity of 585 mAh (g of Sn)$^{-1}$ (0.0901 mAh $cm^{-2}$) in the first cycle. The charge capacity drops dramatically in the following cycles and the discharge capacity increases a little in the subsequent two cycles, then decreases rapidly since 4$^{th}$ cycle. This anode possesses a discharge capacity lower than 100 mAh (g of Sn)$^{-1}$ after 15$^{th}$ cycle. Therefore, on one hand, bare Sn-O-C on flat Cu substrate exhibits really bad performance in contrast to the 3D porous Ni/Sn-O-C thin film anode, it is attributable to the great volume expansion and pulverization of active material Sn during electrochemical cycling. On the other hand, the sharp contrast indicates that three-dimensional highly porous structure can accommodate great volume change of active materials during cycling and maintain stable capacity.

Fig. 5 (c) shows the 1$^{st}$, 2$^{nd}$, 10$^{th}$ and 100$^{th}$ potential profiles of three-dimensional porous nickel supported Sn-O-C composite thin film anode during charge/discharge tests in the potential range between 0.01 V and 1.50 V vs. Li/$Li^+$. In the 1$^{st}$ charge process, the potential sharply drops to 1.85 V with formation of a small pseudo plateau, and gradually drops to 1.7 V with a large plateau (the plateau at about 1.7 V disappears in the following cycles). Then the potential rapidly drops to 0.4 V with a small plateau followed by a gradual decrease to 0.01 V. The plateau at 0.4 V can be clearly observed in the 2$^{nd}$ charge process, however, a pseudo plateau at about 0.3 V and the gradual decrease in potential towards 0.01 V are observed at 10$^{th}$ and 100$^{th}$ cycles. The obvious change in lithiation potential during charge process indicates formation of a series of $Li_xSn$ alloys and SEI film on freshly exposed interface created by mechanical cracking.[20] On the other hand, four pseudo plateaus at about 0.45 V, 0.6 V, 0.7 V and 0.8 V can be observed in the 1$^{st}$ and 2$^{nd}$ discharge process. However, these plateaus can hardly be distinguished and the potential profiles become much more smooth after 10$^{th}$ discharge cycle. Thus, it assumes that the reversible lithiation and delithiation reactions occur in the first several cycles and become irrevisible after 10$^{th}$ cycle, which means the active material Sn can be fully lithiated to the state of $Li_{4.4}Sn$ and be fully delithiated to the original state of Sn in the first several cycles but can never be reverted to the state of Sn after 10$^{th}$ discharge cycle.

The CV profiles of the first four cycles recorded in a potential window of 0.01-1.50 V vs. Li/$Li^+$ at a scan rate of 0.1 mV $s^{-1}$ are shown in Fig. 5 (d). During the 1$^{st}$ charge process, a strong cathodic peak appears at about 1.5V ~ 1.7 V and it disappears after the second cycle, which is consistent with the charge/discharge potential profiles, it is highly possible due to the SEI film formed on the surface of Sn-O-C during



 

electrodeposition. Furthermore, two reduction peaks at about 0.7 V and 0.4 V are observed in the first four cycles in the cathodic branches, which corresponds to the formation of $Li_{0.4}Sn$ and $Li_{2.33}Sn$ alloy, respectively. And the process that potential gradually drops from 0.4 V towards 0.01 V indicates fully lithiation of active material to form $Li_{4.4}Sn$ alloy.[8] On the other hand, four oxidation peaks in the anodic branch at about 0.45 V, 0.6 V, 0.7 V and 0.8 V are observed, which indicates the successive formation of $Li_{2.33}Sn$, LiSn, $Li_{0.4}Sn$ and Sn.[8, 20] Furthermore, both the reduction and oxidation peaks have tendency to become much more smooth and some of them would disappear in the subsequent cycles. In the end, based on the CV analysis of the first four charge/discharge cycles, the assumption that the reversible lithiation and delithiation reactions occur only at first several charge/discharge cycles can be verified.

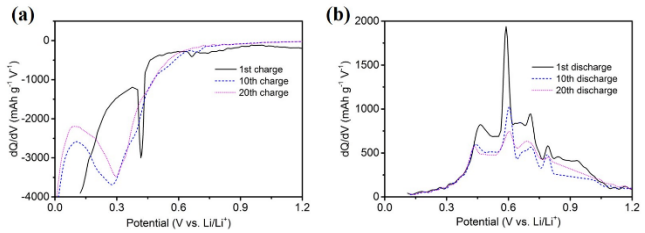


**Fig. 6** (a) Differential capacity curves of the as-prepared 3D porous nickel supported Sn-O-C composite thin film anode at 1st, 10th, 20th cycles during (a) charge and (b) discharge processes.

Differential capacity curves at 1st, 10th and 20th cycles are shown in Fig. 6 to further certify the lithiation and delithiation potential during charge and discharge processes. In Fig. 6 (a), Large sharp peak at 0.4 V and small peak at 0.7 V are observed in the 1st charge process. However, the first peak shifts from 0.4 V to 0.3 V at 10th and 20th cycles, and the second peak at 0.7 V disappears after 20th cycle. The variation tendency of lithiation potential at 0.3 V corresponds well to the result of potential profiles discussed above, and the gradual disappearance of lithiation potential at 0.7 V further certify the assumption that reversible lithiation and delithiation reactions occur only at first several charge/discharge cycles. Peaks at about 0.45 V, 0.6 V, 0.7 V and 0.8 V are observed in the differential capacity curves during the 1st, 10th and 20th discharge processes shown in Fig. 6 (b), but sharp peaks change to broad peaks as cycle number increases, i.e., at 0.7 V and 0.8 V for delithiation. The variation tendency in delithiation potential is consistent with the result of potential profiles, and it also indicates the reversible multi-stage delithiation reactions are gradually replaced by irreversible reactions as cycle number increases.

Fig. 7 shows the impedances of the three-dimensional porous nickel supported Sn-O-C composite thin film anode after different cycles. The impedances are all measured upon reaching a full charge at 0.01 V vs. $Li/Li^+$. All the impedance spectra have similar features: a medium-to-high frequency depressed semicircle and an inclined low frequency line, which corresponds well to the result of previously reported Sn anode.[32, 33] The inclined line in the low frequency region represents the lithium diffusion impedance, and the depressed semicircle suggests overlap between the SEI film and interfacial charge transfer impedance. The results of impedance spectra measured after 5th, 8th, 10th and 50th cycles reveal that total SEI and interfacial charge transfer impedance augments as cycle number increases, which serve as good interpretation of the gradual capacity fading during charge/discharge cycles.

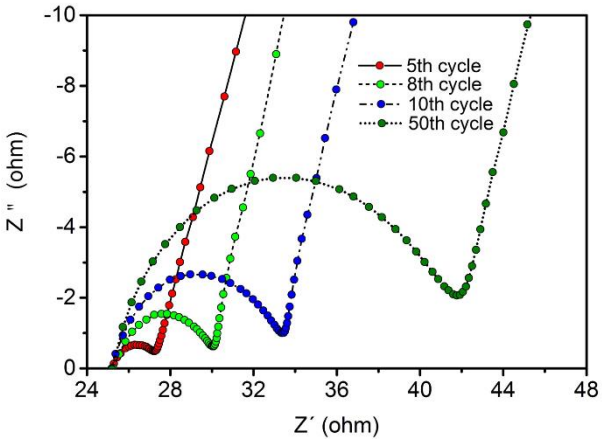


**Fig. 7** Nyquist plots of three-dimensional porous nickel supported Sn-O-C composite thin film anode measured at open circuit voltage upon reaching a full charge at 0.01 V vs. $Li/Li^+$ at 5th, 8th, 10th, 50th cycles.

In order to further understand the relationship between capacity fading and morphology change, the three-dimensional porous nickel supported Sn-O-C composite thin film anode is retained for SEM investigation at first fully lithiated state, first fully delithiated state and 100th fully delithiated state, respectively. Fig. 8 (a) shows SEM image of Sn-O-C composite anode at first fully lithiated state, compared with Fig. 2 (e), obvious volume expansion and dramatic decrease of Ni inter-particle spacings can be observed. The inset graph in Fig. 8 (a) represents magnified SEM image of a Ni particle coated with Sn-O-C composite thin film at fully lithiated state, volume expansion is obvious and small cracks can be found on the surface area, which are consistent with the fully lithiated state of tin with over 300% volume expansion in the first cycle. Fig. 8 (b) shows SEM image of Sn-O-C composite anode at first fully delithiated state, compared with Fig. 8 (a), volume expansion phenomenon disappears and Ni inter-particle spacings recover to initial state but remains a little smaller than that illustrated in Fig. 2 (e). The inset graph in Fig. 8 (b) represents magnified SEM image, great volume compression can be observed comparing with inset graph in Fig. 8 (a), furthermore, many tiny cracks and voids appear on the surface area of Sn-O-C composite anode. Fig. 8 (c) and (d) shows SEM image and its magnified image of Sn-O-C composite anode at fully delithiated state after 100 cycles. Obvious shrinkage in both number and average diameter of pores can be observed in Fig. 8 (c), and the pores seem to be filled to some extent. Despite of small cracks and voids appeared on the surface, the structure integrity is well maintained without pulverization of active materials even after 100 cycles, which accounts for the excellent electrochemical stability during cycling. On the other hand, the appearance of cracks and voids are supposed to be responsible for capacity fading during charge/discharge tests.

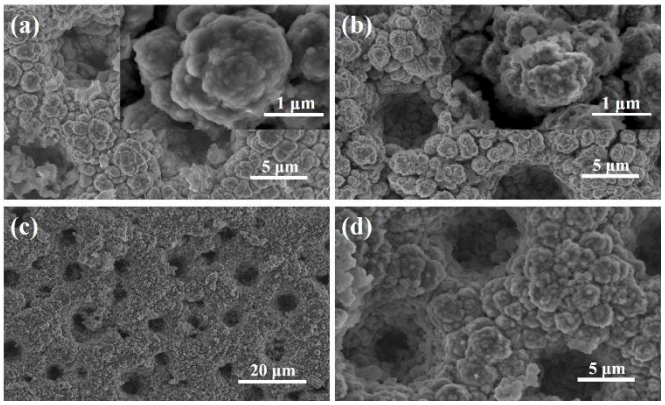


**Fig. 8** Top view SEM images of three-dimensional porous nickel supported Sn-O-C composite thin film anode (a) at fully lithiated state and (b) at fully delithiated state in the first cycle (inset graphs are magnified SEM images); (c) low magnification and (d) high magnification image at fully delithiated state after 100 cycles.

## Conclusions

In summary, a three-dimensional porous nickel supported Sn-O-C composite thin film anode is fabricated by a two-step electrodeposition method. The unique three-dimensional porous structure of Ni offers large surface area, strong mechanical support and high surface roughness, which enables homogeneous electrodeposition of Sn-O-C composite material and reinforce the adhesion strength between active material and substrate. Therefore, the structure integrity of the specially designed electrode could be well maintained during electrochemical cycling process. Furthermore, various characterization methods reveal that the Sn-O-C composite thin film anode is composed of agglomerated Sn nanocrystals inhomogeneously distributed in decomposition products of organic electrolyte and the anode delivers a discharge capacity of 573.4 mAh (g of Sn)$^{-1}$ (0.0883 mAh cm$^{-2}$) after 100 cycles at 0.2 C-rate. Thus, the unique substrate with patterned three-dimensional porous nickel which can realize good adhesion for deposit, ion pass and conductivity, is good technique to apply the Sn-O-C composite thin film to anode of lithium secondary battery, and the electrodeposition method to fabricate anode material also provides a simple, low cost and applicable way for mass production in lithium-ion battery industry.

## Acknowledgements

This work is sponsored by National Natural Science Foundation of China (No. 21303100) and Shanghai Natural Science Foundation (No. 13ZR1420400).

## Notes and references

[a] State Key Laboratory of Metal Matrix Composites, School of Material Science and Engineering, Shanghai Jiao Tong University, No. 800 Dongchuan Rd., Shanghai 200240, China. Fax: +86-21-3420-2748; Tel: +86-21-3420-2748; E-mail: hangtao@sjtu.edu.cn

[b] College of Energy, Xiamen University, Xiamen City, Fujian Province, 361102, China. Fax./Tel: +86-0592-2185278; E-mail: gran@xmu.edu.cn

1. M. Armand and J.-M. Tarascon, *Nature*, 2008, 451, 652-657.
2. C. Liu, F. Li, L.-P. Ma and H.-M. Cheng, *Advanced Materials*, 2010, 22, E28-E62.
3. M. Wachtler, J. O. Besenhard and M. Winter, *Journal of Power Sources*, 2001, 94, 189-193.
4. L. Ji, Z. Tan, T. Kuykendall, E. J. An, Y. Fu, V. Battaglia and Y. Zhang, *Energy Environ. Sci.*, 2011, 4, 3611-3616.
5. S. Brutti, J. Hassoun, B. Scrosati, C.-Y. Lin, H. Wu and H.-W. Hsieh, *Journal of Power Sources*, 2012, 217, 72-76.
6. Z. Du, S. Zhang, Y. Xing and X. Wu, *Journal of Power Sources*, 2011, 196, 9780-9785.
7. X. Chen, J. Guo, K. Gerasopoulos, A. Langrock, A. Brown, R. Ghodssi, J. N. Culver and C. Wang, *Journal of Power Sources*, 2012, 211, 129-132.
8. D. H. Nam, R. H. Kim, D. W. Han and H. S. Kwon, *Electrochim. Acta*, 2012, 66, 126-132.
9. N. Tamura, R. Ohshita, M. Fujimoto, S. Fujitani, M. Kamino and I. Yonezu, *Journal of Power Sources*, 2002, 107, 48-55.
10. H. Mukaibo, T. Sumi, T. Yokoshima, T. Momma and T. Osaka, *Electrochemical and Solid State Letters*, 2003, 6, A218-A220.
11. J. Hassoun, G. A. Elia, S. Panero and B. Scrosati, *Journal of Power Sources*, 2011, 196, 7767-7770.
12. X. L. Wang, H. Y. Chen, J. M. Bai and W. Q. Han, *J. Phys. Chem. Lett.*, 2012, 3, 1488-1492.
13. M. Winter and J. O. Besenhard, *Electrochim. Acta*, 1999, 45, 31-50.
14. H. Nara, Y. Fukuhara, A. Takai, M. Komatsu, H. Mukaibo, Y. Yamauchi, T. Momma, K. Kuroda and T. Osaka, *Chemistry Letters*, 2008, 37, 142-143.
15. I. Grigoriants, B. Markovsky, R. Persky, I. Perelshtein, A. Gedanken, D. Aurbach, B. Filanovsky, T. Bourenko and I. Felner, *Electrochim. Acta*, 2008, 54, 690-697.
16. X. W. Lou, Y. Wang, C. Yuan, J. Y. Lee and L. A. Archer, *Advanced Materials*, 2006, 18, 2325-2329.
17. Z. Chen, Y. Cao, J. Qian, X. Ai and H. Yang, *Journal of Materials Chemistry*, 2010, 20, 7266-7271.
18. F. S. Ke, L. Huang, L. Jamison, L. J. Xue, G. Z. Wei, J. T. Li, X. D. Zhou and S. G. Sun, *Nano Energy*, 2013, 2, 595-603.
19. M. Jeong, H. Nara, T. Yokoshima, T. Momma and T. Osaka, 2012.
20. T. Momma, M. Jeong, T. Yokoshima, H. Nara, A. Toyoda and T. Osaka, *Journal of Power Sources*, 2013, 242, 527-532.
21. M. Jeong, T. Yokoshima, H. Nara, T. Momma and T. Osaka, *Journal of The Electrochemical Society*, 2014, 161, D3025-D3031.
22. M. Jeong, T. Yokoshima, H. Nara, T. Momma and T. Osaka, *RSC Adv.*, 2014, 4, 26872-26880.
23. M. Jeong, T. Yokoshima, H. Nara, T. Momma and T. Osaka, *Journal of Power Sources*, 2015, 275, 525-530.
24. H. C. Shin, J. Dong and M. Liu, *Advanced Materials*, 2003, 15, 1610-1614.
25. H. C. Shin, J. Dong and M. Liu, *Advanced Materials*, 2004, 16, 237-240.
26. Y. Q. Zhang, X. H. Xia, X. L. Wang, Y. J. Mai, S. J. Shi, Y. Y. Tang, C. G. Cu and J. P. Tu, *Journal of Power Sources*, 2012, 213, 106-111.
27. D. Youb âKim and D. Wook âKim, *J. Mater. Chem. A*, 2014, 2, 2478-2481.
28. X. Qian, T. Hang, H. Nara, T. Yokoshima, M. Li and T. Osaka, *Journal of Power Sources*, 2014, 272, 794-799.
29. C. K. Chan, R. Ruffo, S. S. Hong and Y. Cui, *Journal of Power Sources*, 2009, 189, 1132-1140.
30. D. Aurbach, A. Nimberger, B. Markovsky, E. Levi, E. Sominski and A. Gedanken, *Chemistry of Materials*, 2002, 14, 4155-4163.
31. T. Momma, S. Aoki, H. Nara, T. Yokoshima and T. Osaka, *Electrochem. Commun.*, 2011, 13, 969-972.
32. X. Zhao, Z. Xia and D. Xia, *Electrochim. Acta*, 2010, 55, 6004-6009.
33. F. Nobili, M. Mancini, S. Dsoke, R. Tossici and R. Marassi, *Journal of Power Sources*, 2010, 195, 7090-7097.



 